

Journal of Materials Chemistry A

Accepted Manuscript



This is an *Accepted Manuscript*, which has been through the Royal Society of Chemistry peer review process and has been accepted for publication.

Accepted Manuscripts are published online shortly after acceptance, before technical editing, formatting and proof reading. Using this free service, authors can make their results available to the community, in citable form, before we publish the edited article. We will replace this *Accepted Manuscript* with the edited and formatted *Advance Article* as soon as it is available.

You can find more information about *Accepted Manuscripts* in the [Information for Authors](#).

Please note that technical editing may introduce minor changes to the text and/or graphics, which may alter content. The journal's standard [Terms & Conditions](#) and the [Ethical guidelines](#) still apply. In no event shall the Royal Society of Chemistry be held responsible for any errors or omissions in this *Accepted Manuscript* or any consequences arising from the use of any information it contains.

SnO₂ Nanowire anchored Graphene nanosheet matrix for the superior performance of Li-ion thin film battery anode

1. Introduction

Lithium ion batteries (LIBs) are crucial systems for the energy storages in electronic devices such as communication/portable devices, electric/hybrid vehicles and other power gadgets etc. LIBs offer many advantages over other battery systems like high energy density and high voltage, high charge capacity and stability, large cyclability and rate capability [1,2]. The electrode materials play an important role in the performance of lithium batteries. Many advances have to be made to meet today's increasing demands in high energy density and high cycle rate by designing new nanomaterials and processing techniques. Current commercial Li ion battery largely depends on graphite as the anode. It can be reversibly charged and discharged under intercalation potentials with reasonable specific capacity, but the low theoretical capacity (372mAh/g) of graphite prevents the use of LIBs for high energy and high power applications [3].

The developments of all solid state thin film batteries (TFB) are essential for miniaturization of portable electronic devices and to avoid the problems caused by liquid electrolyte. A thin film battery is composed of several electrochemical cells that are connected in series and/or in parallel to provide the required voltage and capacity. All solid state (micro batteries) is essential for the state of art microelectronic and portable electronic devices. The energy and power requirement for these devices are ever increased and leads to research into novel battery structure and electrode materials with increased volume energy and power density [4,5]. Due to its thinner dimension, TFBs have greater applications in making thinner electronic devices, RFID tags, wireless sensors and implantable medical devices [6,7]. These batteries exhibit the same voltage

and current as their bulky counterparts. The advancement of nanotechnology and cell engineering brought TFBs to achieve high energy density and cycle life.

Thin film batteries are built layer by layer by vapour deposition. There are various methods being used to deposit thin film electrode materials onto the current collector such as, sputtering, CVD and sol gel methods [8]. Plasma based materials deposition techniques are well suitable for the industrial applications. Multiple thin film cells can reduce the footprint of large planar battery area; will be a solution to attain large energy and power requirements. The first solid state thin film battery was developed by Hitachi Co., Japan in 1982 [9]. Thin film battery with more stable LIPON as the solid electrolyte was developed by a group at Oak ridge national laboratory [10]. There are several companies and research institutions actively involved to develop the better thin film battery systems [8]. J H Pikal et al [11] demonstrates 3-D micro batteries from bi-continues nano porous electrodes that gave the power density of $7.4 \text{ mWcm}^{-2}\mu\text{m}^{-1}$. Graphene (having a high theoretical specific surface area of $2630 \text{ m}^2\text{g}^{-1}$) or carbon nano structures can enhance the storage capacity by several orders [12]. Graphene can accommodate Li ions on both sides. This makes the theoretical capacity two times larger than ($\sim 740 \text{ mAhg}^{-1}$) that of other carbon materials.

In order to increase the battery's capability, various elements or compounds (eg. Si, Sn, Ge, SnO_2 etc) are alloyed to lithium to get much larger specific capacities than commercial graphite. Among the various metal and metal oxide based electrodes, both tin (Sn) and tin oxide (SnO_2) [13,14] have been discussed as the important anode materials for Li-ion batteries, because of their semiconducting properties combined with high capacity (Sn, 994 mAhg^{-1} and SnO_2 781 mAhg^{-1}) compared to that of graphite [15]. However, significant capacity fading with cycling is a

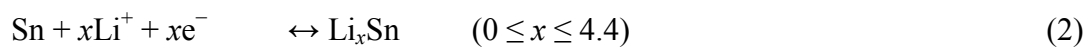
problem specifically with metal oxide based materials due to large volume changes during Li alloying and dealloying, which leads to metal segregation, crystallographic deformation [16] and agglomeration of active materials. In the case of Sn, the volume changes are as high as 259% [17].

The huge volume changes associated with lithiation/delithiation process is a major drawback for SnO₂ based electrodes and hindering it from real applications [18]. In order to solve the issues associated with metal oxide materials, various nano structured SnO₂ and SnO₂ composites have been proposed. These can be accommodating the volume changes during the cyclic process. Nanostructured electrode materials possess many advantages, such as increased number of electrochemical active sites and better control over stress due to lithiation/delithiation process [19, 20]. Nanostructured metal oxide particles with homogeneous carbon coating have already been reported to improve the mechanical and electrochemical stability [21]. The carbon support on nanoparticles enables a better accommodation of the large volume change and improves the electron conductivity of electrode [22]. The nano carbon materials often gave high columbic efficiencies and cycle life, but the volumetric energy density and rate performance were poor due to the formation of large SEI film [23]. By using nanostructured inorganic materials, the rates of the electron and counter ion transport are increased. The transport properties have been improved somewhat by using nano-architected electrodes with large surface areas [24].

Nanowires and nanoparticles of alloy materials are better choice for advanced Li batteries. The transport of Li ions is one of the main issues that give rise to current limitations. Engineering the active materials into exceptional nano architectures will enhance the efficiency of the

electrochemical performance such as specific capacity, rate capabilities and cycling stability [25]. Several studies show that SnO₂ nanowire/ heterostructures gave a capacity of ~700mAh/g up to 15 cycles [26] then fade to ~300mAh/g after 50 cycles. Kim et al demonstrated stable cycling behaviour for SnO₂ nanowire electrode which delivered a high specific discharge capacity of 510 mAh/g [27]. Graphene nanosheet (GNS) matrix having flexible two-dimensional structure, high surface area (over 2600 m² g⁻¹), excellent electrical conductivity and the ability to diminish the stress of electrode upon cycling will support the SnO₂ based nanostructures [28, 29].

In our study we are aiming for the higher electrochemical performance of SnO₂NW@GNS anode by adding the advantage of both materials vs graphene nanosheet and SnO₂ nano wire. We have modified the carbon into graphene nanosheet (GNS) matrix and nanowires of SnO₂ were embedded on it (SnO₂NW@GNS). GNS consists of few layers of graphene grown vertically over the substrate and provides very high porosity. The high surface area of GNS able to attach more SnO₂ nanowire on to the wall of graphene sheet, thus ease for the Li ion migration in to the active materials. Hence tailoring the structure of SnO₂ materials or embedded on carbon matrices will enhancing the SnO₂NW@GNS anode performance. It is well known that the following equations are involved in the SnO₂ based anodes.



The first reaction is considered as irreversible and is responsible for the irreversible capacity loss from first to second discharge cycles [30, 31]. But this irreversible capacity could also become

reversible for nanometer-sized SnO₂ nano particles or wires [32]. The second equation is widely known for the reversible capacity, in which Li is continuously alloying with Sn [33]. These kinds of nano architectures of carbon are very much suitable for energy storage applications.

2. Experimental

2.1. Synthesis of graphene nanosheet and SnO₂ nanowire

Graphene nanosheet (GNS) was synthesized on Cu substrate using plasma enhanced (electron cyclotron resonance) ECR-CVD. In this method Acetylene (C₂H₂) was decomposed to graphene nanosheet in the presence of microwave plasma. The details of GNS synthesis have been given in our previous report [34]. For the growth of SnO₂ nano wires, a thin layer of about 3nm gold has been sputtered over GNS sample as the catalyst. Then the gold coated GNS sample was annealed at 600⁰C for 10 minutes. Gold particles of approximately 5nm in size were formed over GNS after annealing. These spherical particles serve as catalyst for growing individual SnO₂ nanowires. On these samples SnO₂ was deposited by reactive electron beam evaporation of Sn in the presence of oxygen. Prior to the evaporation of Sn, the substrate temperature was kept at 620⁰C and the deposition rate of Sn was about 1.4 Å/s. The oxygen partial pressure was maintained at 4×10⁻⁴mbar and the deposition was carried out for 15 minutes. The nanowire growth will take place at very low evaporation rate of Sn. The total active material deposited over 1.13 cm² area of copper substrate weighed about 0.1mg (including the weight of GNS and SnO₂ nanowire). The mass of SnO₂ deposited (about 100nm thickness) was determined using density calculation was about 7.85×10⁻⁵g as against the mass of GNS which is about 2.15×10⁻⁵ g.

2.2. Characterization of SnO₂NW@GNS film

The surface morphologies of GNS and nanowire were characterized by field emission scanning electron microscopy (FESEM, ULTRA 55, Karl Zeiss). The x-ray diffraction (XRD, Rigaku Smartlab) pattern of the nanowire@GNS sample was obtained with Cu K α radiation source. The surface chemistry and bonding nature of the sample was analyzed with x-ray photoelectron spectroscopy (XPS, SPECS GmbH, Phoibos 100 MCD Energy Analyzer using Mg-K α radiation, 1283.6eV) and Raman spectrometer (LabRAM HR spectrometer with an Ar-ion laser of wavelength of 514 nm, at a magnification of 100 \times and a CCD camera detector). The high resolution TEM (HRTEM, FEI TECHNAI T20 microscope operated at 200 kV) was performed for the pristine sample and after electrochemical performance.

2.3. Electrochemical measurements

All electrochemical testing was done in Swagelok cells with 1M LiPF₄ I EC/DMC (1:1 w/w) as the electrolyte (EC= ethylene carbonate, DMC= dimethyl carbonate) and Li foil as the counter and reference electrode. The SnO₂NW@GNS over copper substrate was used as the anode electrode. Cells were assembled as half cell configuration in Ar-filled MBraun glove-box model Unilab to avoid the contamination and oxidation. The total weight of the active material was accurately measured by subtracting the mass of the sample before and after the deposition using a microbalance. We calculated the total capacity from the weight of composite. The Cells were galvanostatically charged and discharged at various current densities using a CHI 665 electrochemical work station within the potential range of 2–0.1 V (vs. Li/Li⁺) at ambient temperature. Cyclic voltammetry (CV) was performed between 2.0 and 0.1 V at a scan rate of 0.5 mVs⁻¹. Various current densities were used to study the rate capacity of SnO₂NW@GNS electrode.

3. Results and discussion

The morphology of highly porous, vertically oriented graphene nanosheet film grown over copper substrate is shown in fig. 1a. Each wall of graphene sheet is a combination of several single graphene sheets. This porous structure of GNS gives high surface to volume ratio and very much suitable for maximum Li storage. The Li-ions can attach to the both sides of the graphene wall. Fig. 1b gives the raman spectrum of GNS thin film. The 2d peak at 2700 cm^{-1} shows the presence of many graphene layers. Very thin film of gold coated over the GNS sample is shown in fig. 1c. After annealing at 600°C , the spherical particles of gold were attached to the wall of GNS and these gold particles act as the sites for SnO_2 nanowire growth. Fig. 1d shows the SnO_2 nanowire on GNS ($\text{SnO}_2\text{NW@GNS}$) after the initial growth stage (after 10 minutes of deposition) and it can be seen that the wires were attached to the graphene wall.

Fig. 2a shows a typical field emission scanning electron microscopy (FESEM) image of as synthesized SnO_2 nanowire grown over GNS matrix with Au catalyst at a substrate temperature of 620°C . The total time taken for the deposition of SnO_2 nanowire was about 30 minutes. The long nanowires of SnO_2 are seen in the porous structure of GNS matrix. The wires are uniformly distributed over GNS matrix. A cross section SEM image of $\text{SnO}_2\text{NW@GNS}$ is shown in fig. 2b. All the nanowires are seen with a tip on the top (white circles on the cross section image) and were assumed to be the eutectic metal alloy, indicating that the nanowires were grown via tip-led growth according to VLS mechanism [35].

The XRD pattern of $\text{SnO}_2\text{NW@GNS}$ electrode is shown in supporting information (fig. S1). The peaks marked in the spectra are well matched with the rutile- tetragonal SnO_2 phase (space group $p4_2/mnm$). A broad peak at $2\theta=21^{\circ}$ was assigned to the graphitic peak coming from GNS matrix.

Fig. 2c shows the transmission electron microscopy image of SnO₂NW@GNS. The wires seem to arise from the graphene sheet (darker side of the image) with a eutectic metal alloy at the tip of each wire. An energy-dispersive (EDS) line scan of individual nano wire from the tip along the nanowire stem indicated that the tip of the metal alloy was abundant of catalyst, gold, whereas the nanowire stem consist of pure SnO₂ without any presence of Au on it (supporting info. Fig. S2). The HRTEM of single nanowire of SnO₂ confirmed that the as synthesized wires are highly- ordered and single crystal phase with sharp periodic lattice fringed. Each nanowire is very thin with diameter of ~10 to 5 nm. The SAED pattern (inset of fig. 2d) shows that the nanowires are with a preferential growth direction of [101]. The inter-atomic plane distance calculated to (101) lattice was 2.56Å.

XPS measurements were performed for the electrodes before and after the electrochemical studies. Fig. 3a and b show the survey spectrum and high resolution spectrum of Sn 3d_{5/2} before performing the electrochemical studies. The spectrum of Sn3d_{5/2} was de-convoluted into two peaks at 486.7 eV and 484.8 eV for SnO₂ and metallic Tin, respectively. A small percentage of metallic tin might have deposited during deposition.

3.1. Electrochemical analysis

Fig. 4a shows the cyclic voltammetry (CV) curve of first two cycles of SnO₂NW@GNS at a scan rate of 0.05mV/s in the potential range from 0.01 to 2.0 V. The first scan of fig. 4a shows a broad peak in the range of 0.8 to 1.2V and a sharp peak at 0.8 V arises from the broad peak. The broad peak may be attributed to the formation of SEI with graphene sheet. The broad peak in the same range is also visible in CV of GNS (grapheme nanosheet) film alone on copper substrate (fig. S3, supporting info.). A small peak at ~1.0V (fig. 4a) can be assigned to the conversion of SnO₂ to

SnO and Li₂O [36, 37], whereas, the sharp peak at 0.8V (fig. 4a) is attributed to the conversion of SnO₂ to Sn and Li₂O and the formation of SEI. The CV measurement of GNS electrode demonstrates that the Li ion could intercalate and deintercalate into the graphene sheets. The Li insertion/deintercalation takes place at ≤ 0.1 V in the graphene sheets. The lithium ion insertion potential is quite low, which is very close to 0 V vs the Li/Li⁺ reference electrode, whereas, the potential for lithium ion deintercalation is in the range 0.2- 0.3 V [38].

Fig. 4b and c show galvanostatic charge-discharge cycles and rate capability of SnO₂NW@GNS electrode. The first discharge and charge capacities are 1335 mAh/g and 4930 mAh/g, respectively at a current density of 23 μ A/cm². The total capacity is from the contributions of SnO₂ nanowire and graphene nanosheet. The much higher charge capacity is due to the GNS matrix. High degree of defects in GNS may act as the Li ion sites that contributed more capacity. A large irreversible capacity loss of about 3600 mAh/g (73%) observed for the sample at first cycle. This huge irreversible capacity loss is due the irreversible reduction of SnO₂ to Sn as described in equ. 1 and other irreversible process such as decomposition of electrolyte [39, 40]. During second cycle, 64% of charge capacity retained for the discharge capacity, which is 1240 mAh/g. Subsequent discharge cycles obtained 67% and 75% of charge capacities. On the first charge, a flat plateau appeared around 0.8V, which was attributed to the SEI formation. The charge-discharge profiles of SnO₂ nanowire on copper substrates is given in S4 (supporting info.). The first charge and discharge capacities were obtained as 2169 mAhg⁻¹ and 828 mAhg⁻¹ respectively, at a current density of 23 μ A/cm². About 62% of irreversible capacity loss was observed in the first cycle which is less than that of SnO₂NW@GNS electrode.

During the second cycle, about 89% of charge capacity retained for the discharge capacity. Only first cycles of charge-discharge capacities of various current densities were given in fig S5 of supporting information. The irreversible decomposition of SnO₂ to the metallic Tin surrounded by an amorphous, inactive Li₂O matrix was ascribed to the SEI [41, 42]. The amorphous Li₂O matrix allows Li ions diffuse through and prevent the agglomeration of Sn atoms or Li_xSn alloy regions during volume changes [43]. The rate performance of electrode was evaluated at various current densities from 23 μA/cm² to 177 μA/cm². A coulombic efficiency of ~87% was obtained for SnO₂NW@GNS electrode after 50 cycles at a current density of 23 μA/cm² (fig. 4d).

3.2. XPS and TEM studies after electrochemical performance

The xps spectra corresponding to Sn 3d_{5/2} and Li 1s after the first charge cycle and discharge cycle are shown in fig. 5a &c and fig. 5 b&d, respectively. After first charge, the spectra show a peak at 486.7 eV that can be attributed to the SnO₂ phase. The Li 1s peak at 56.7 gives a Li₂O phase of lithium. An alloy of SnO₂ with Li may form and still retain some crystallinity. These have been confirmed from the TEM of the sample after the first charge cycle (fig. 6b).

A broad peak of Sn 3d_{5/2} is observed after the first discharge cycle (fig.5c). The peaks observed at 485.3 eV and 486.7 eV are assigned to Sn and Sn⁴⁺, respectively. The corresponding Li 1s peak also de-convoluted to two peaks at 54.6 and 56.3 (fig. 5d) attributed to metallic lithium and Li₂O phase, respectively. The Li₂O is an amorphous phase which allows Li-ions pass through it and electrically insulating. XPS spectra of the electrode after 50th cycle have given in supporting information (S6).

In order to understand the modifications that occur in the electrode during charge/discharge process, an additional TEM study was carried out for electrode after the charge cycle (after first

lithiation) and after the discharge cycle (after first delithiation). Fig. 6a and b show the TEM images of electrodes after the first charges state. The nanowire morphology of SnO₂ was largely distorted and even mild structure of nanowire can be seen in the TEM image (fig. 6a). During charging, the formation of Li₂O results in large volume expansion in the nanowire [44]. The high resolution TEM image of the electrode shows clear nanowire morphology and the SAED pattern (inset of fig. 6b) shows retention of some degree of crystallinity the nanowire during the first charged state. The lattice fringes have been changed when compared to the original SnO₂ nanowire shown in fig. 2d. After the discharge cycle, the complete morphology of SnO₂ nanowire undergoes significant change and nanoparticles of Tin have formed (fig. 6c). The HRTEM of tin particles shows crystalline nature and having the sizes of 5-10 nm. In the discharge process, the Li₂O did not take part in electrochemical lithiation process and only Li_xSn nanoprecipitates were active in lithiation process.

4. Conclusions

In summary, a 3-D heterogeneously nanostructured thin film was designed by uniformly anchoring SnO₂ nanowires on the surface of GNS matrix. This nano composite exhibited superior electrochemical performance which, we attributed due to the morphology of the wire and GNS matrix. The one dimensional wire attached to the side walls of GNS film and increases the surface area of active material for Li diffusion. Discharge capacity obtained was about 1335 mAhg⁻¹ and the columbic efficiency of ~86% after the 50th cycle. Our studies show the potential opportunity for developing high-performance Li-ion batteries based on the GNS architecture composite. The present architecture of anode material provides the concept of 3-D micro batteries. Stable 3-D framework of GNS supports SnO₂ NWs without agglomeration, while graphene sheets play an important role in enhancing the conductivity of the electrode.

References

- [1] V. Etacheri, R. Marom, R. Elazari, G. Salitra and D. Aurbach, *Energy Environ. Sci.*, 2011, **4**, 3243.
- [2] R. Marom, S. F. Amalraj, N. Leifer, D. Jacob and D. Aurbach, *J. Mater. Chem.*, 2011, **21**, 9938.
- [3] Y. Idota, T. Kubota, A. Matsufuji, Y. Maekawa and T. Miyasaka, *Science*, 1997, **276**, 1395.
- [4] J. B. Bates, G. R. Gruzalski, N. J. Dudney, C. F. Luck and X. H. Yu, *Solid State Ionics*, 1994, **70**, 619.
- [5] J. B. Bates, N. J. Dudney, D. C. Lubben, G. R. Gruzalski, B. S. Kwak, X. H. Yu and R. A. Zuhr, *J. of Power Sources*, 1995, **54**, 58.
- [6] H. Nishide and K. Oyaizu, *Science*, 2008, **319**, 737.
- [7] A. Nathan, A. Ahnood, M. T. Cole, S. Lee, Y. Suzuki, P. Hiralal, F. Bonaccorso, T. Hasan, L. G. Gancedo, A. Dyadyusha, S. Haque, P. Andrew, S. Hofmann, J. Moultrie, D. Chu, A. Flewitt, A. Ferrari, M. Kelly, J. Robertson, G. Amaratunga and W. Milne, *Proc. IEEE*, 2012, **100**, 1486.
- [8] A. Patil, V. Patil, D. W. Shin, J. W. Choi, D. S. Paik and S. J. Y. Stacking, *Materials Research Bulletin*, 2008, **43**, 1913.
- [9] K. Kanehori, K. Matsumoto, K. Miyauchi and T. Kudo, *Solid State Ionics*, 1983, **9–10**, 1445.
- [10] X. Yu, J. B. Bates, G. E. Jellison and F. X. Hart, *J. Electrochem. Soc.*, 1997, **144**, 524.
- [11] J. H. Pikul, H. G. Zhang, J. Cho, P. V. Braun and W. P. King, *Nature Communications*, 2013, **4**, 1732.
- [12] N. Mahmood, C. Zhang, H. Yin and Y. Hou, *J. Mater. Chem. A*, 2014, **2**, 15.
- [13] X. Song, J. Pan, L. Xiao, L. Gao and S. Mathur, *Nanotechnology*, 2013, **24**, 205401.
- [14] E. Kim, D. Son, T. G. Kim, J. Cho, B. Park, K. S. Ryu and S. H. Chang, *Angew. Chem., Int. Ed.*, 2004, **43**, 5984.
- [15] M. Winter and J. O. Besenhard, *Electrochim. Acta*, 1999, **45**, 31.
- [16] M. Wachtler, M. Winter and J. O. Besenhard, *J. Power Sources*, 2007, **105**, 151.
- [17] B. A. Boukamp, G. C. Lesh and R. A. Huggins, *J. Electrochem. Soc.*, 1981, **128**, 725.
- [18] X. W. Lou, Y. Wang, C. Yuan, J. Y. Lee and L. A. Archer, *Adv. Mater.*, 2006, **18**, 2325- 2329.
- [19] C. K. Chan, H. L. Peng, G. Liu, K. McIlwrath, X. F. Zhang, R. A. Huggins and Y. Cui, *Nat. Nanotechnol.*, 2008, **3**, 31.
- [20] A. Magasinski, P. Dixon, B. Hertzberg, A. Kvit, J. Ayala and G. Yushin, *Nat. Mater.*, 2010, **9**, 353.
- [21] J. W. Zhu, S. Chen, X. D. Wu, Q. F. Han and X. Wang, *ACS Nano*, 2010, **4**, 2822.
- [22] M. S. Park, Y. M. Kang, J. H. Kim, G. X. Wang, S. X. Dou and H. K. Liu, *Carbon*, 2008, **46**, 35.
- [23] J. Hassoun, F. Bonaccorso, M. Agostini, M. Angelucci, M.G. Betti, R. Cingolani, M. Gemmi, C. Mariani, S. Panero, V. Pellegrini, and B. Scrosati, *Nano Lett.*, 2014, **14** (8), 4901.
- [24] H. Nishide and K. Oyaizu, *Science*, 2008, **319**, 737.
- [25] A. R. Kamali and D. J. Fray, *Rev. Adv. Mater. Sci.*, 2011, **27**, 14.

- [26] D. W. Kim, I. S. Hwang, S. J. Kwon, H. Y. Kang, K. S. Park, Y. J. Choi, K. J. Choi and J. G. Park, *Nano Lett.*, 2007, **7**, 3041.
- [27] Y. D. Ko, J. G. Kang, J. G. Park, S. Lee and D. W. Kim, *Nanotechnology*, 2009, **20**, 455701
- [28] S. M. Paek, E. J. Yoo and I. Honma, *Nano Lett.*, 2009, **9**, 72.
- [29] J. Yao, X. P. Shen, B. Wang, H. K. Liu and G. X. Wang, *Electrochem. Commun.*, 2009, **11**, 1849.
- [30] J. O. Besenhard, J. Yang and M. Winter, *J. Power Sources*, 1997, **68**, 87.
- [31] O. Mao, R. A. Dunlap and J. R. Dahn, *J. Electrochem. Soc.*, 1999, **146**, 405.
- [32] Z. Chen, M. Zhou, Y. Cao, X. Ai, H. Yang and J. Liu, *Adv. Energy Mater.*, 2012, **2**, 95.
- [33] M. S. Park, G. X. Wang, Y. M. Kang, D. Wexler, S. X. Dou and H. K. Liu, *Angew. Chem. Int. Ed.*, 2007, **46**, 750.
- [34] R. Thomas, K. Y. Rao and G. M. Rao, *Electrochemi. Acta*, 2013, **108**, 458.
- [35] Y. Y. Wu and P. D. Yang, *J. Am. Chem. Soc.*, 2001, **123**, 3165.
- [36] D. Wang, R. Kou, D. Choi, Z. Yang, Z. Nie, J. Li, L. V. Saraf, D. Hu, J. Zhang, G. L. Graff, J. Liu, M. A. Pope and I. A. Aksay, *ACS Nano*, 2010, **4**, 1587.
- [37] W. Shi, J. Zhu, D. H. Sim, Y. Y. Tay, Z. Lu, X. Zhang, Y. Sharma, M. Srinivasan, H. Zhang, H. H. Hng, Q. Yan, *J. Mater. Chem.*, 2011, **21**, 3422.
- [38] A. Kumar, A. L. M. Reddy, A. Mukherjee, M. Dubey, X. Zhan, N. Singh, L. Ci, W. E. Billups, J. Nagurny, G. Mital, and P. M. Ajayan, *ACS Nano*, 2011, **5**, 4345.
- [39] X. W. Lou, D. Deng, J. Y. Lee and L. A. Archer, *Chem. Mater.* 2008, **20**, 6562.
- [40] M. S. Park, G. X. Wang, Y. M. Kang, D. Wexler, S. X. Dou and H. K. Liu, *Angew. Chem., Int. Ed.* 2007, **46**, 750.
- [41] I. A. Courtney and J. R. Dahn, *J. Electrochem. Soc.*, 1997, **144**, 2045.
- [42] M. S. Park, G. X. Wang, Y. M. Kang, D. Wexler, S. X. Dou, H. K. Liu, *Angew. Chem.* 2007, **119**, 764.
- [43] A. Sivashanmugam, T. P. Kumar T, N. G. Renganathan, S. Gopukumar, M. M. Wohlfahrt and J. Garche, *Journal of Power Sources*, 2005, **144**, 197.
- [44] J. Y. Huang, L. Zhong, C. M. Wang, J. P. Sullivan, W. Xu, L. Q. Zhang, S. X. Mao, N. S. Hudak, X. H. Liu, A. Subramanian, H. Fan, L. Qi, A. Kushima and J. Li, *Science*, 2010, **330**, 1515.

Figure 1

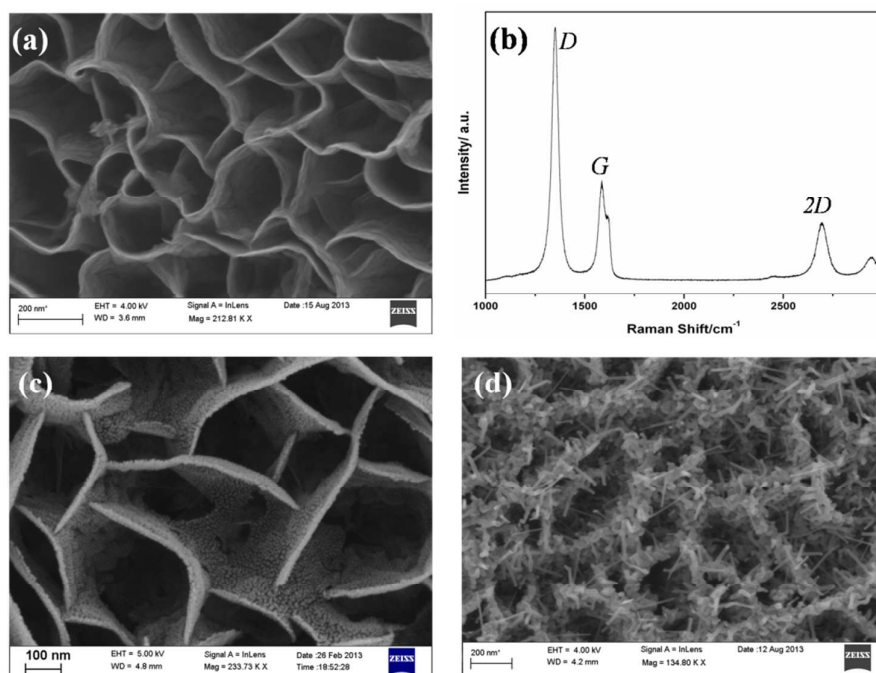


Fig. 1 (a) Scanning electron microscopy image (SEM) graphene nanosheet (GNS) on copper substrate, (b) raman spectrum of GNS, SEM image of (c) Gold deposited over GNS and (d) early stages of growth of SnO₂ nanowire.

Figure 2

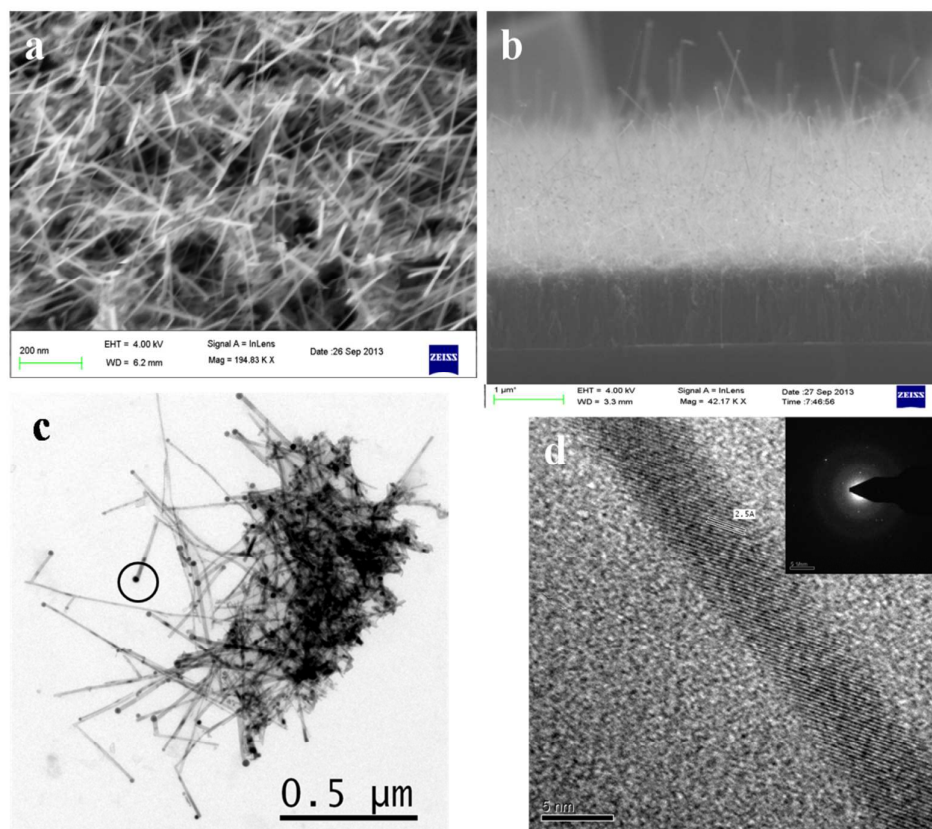


Fig. 2 (a) FESEM image of SnO₂ nanowire (b) cross section SEM image of SnO₂ nanowire on GNS, (c) TEM image of SnO₂NW@GNS nanowire and (d) HRTEM of single nanowire (inset) SAED pattern

Figure 3

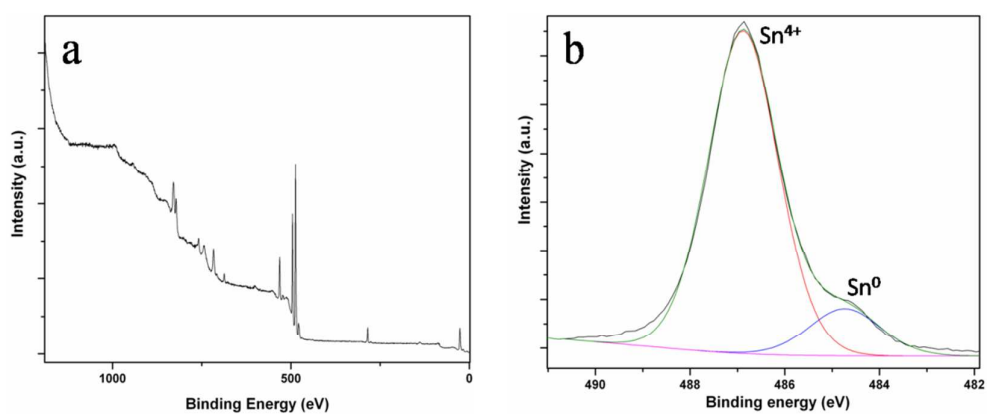


Fig. 3 XPS spectra of SnO₂NW@GNS electrodes before electrochemical cycles (a) survey scan of electrode, (b) High resolution spectrum of Sn 3d_{5/2}

Figure 4

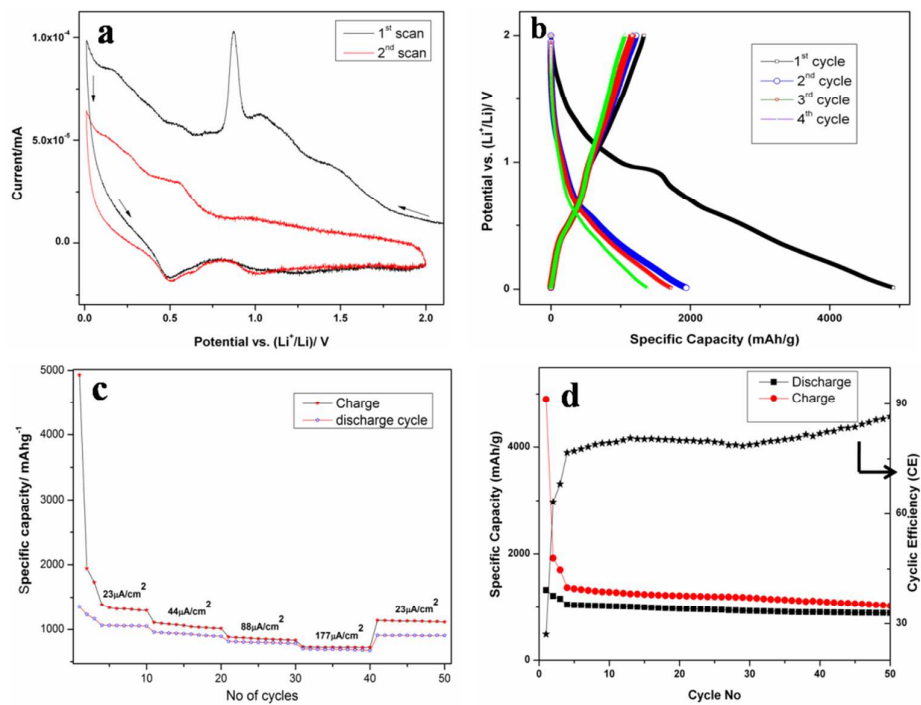


Fig. 4 (a) Cyclic Voltammetry of SnO₂NW@GNS (b) Galvanostatic charge/discharge profile of SnO₂NW@GNS, (c) Rate performance of SnO₂NW@GNS electrode and (d) coulombic efficiency versus cycle number of SnO₂NW@GNS electrode.

Figure 5

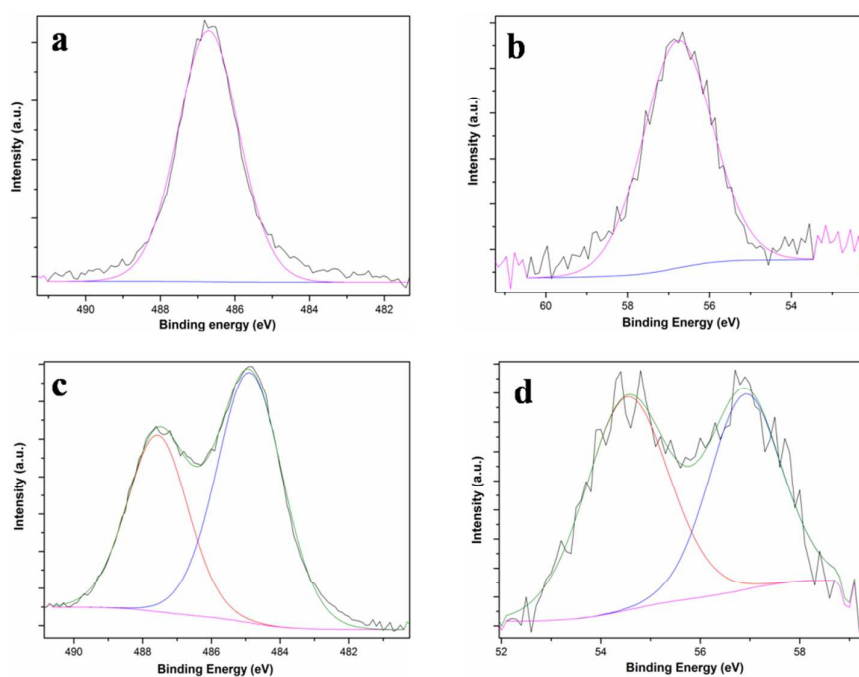


Fig. 5 XPS spectra of SnO₂NW@GNS electrodes after electrochemical cycles (a) and (b) High resolution spectrum of Sn 3d_{5/2} and Li 1s after first charge cycle, (c) and (d) Sn 3d_{5/2} and Li 1s spectrum after first discharge cycle, respectively.

Figure 6

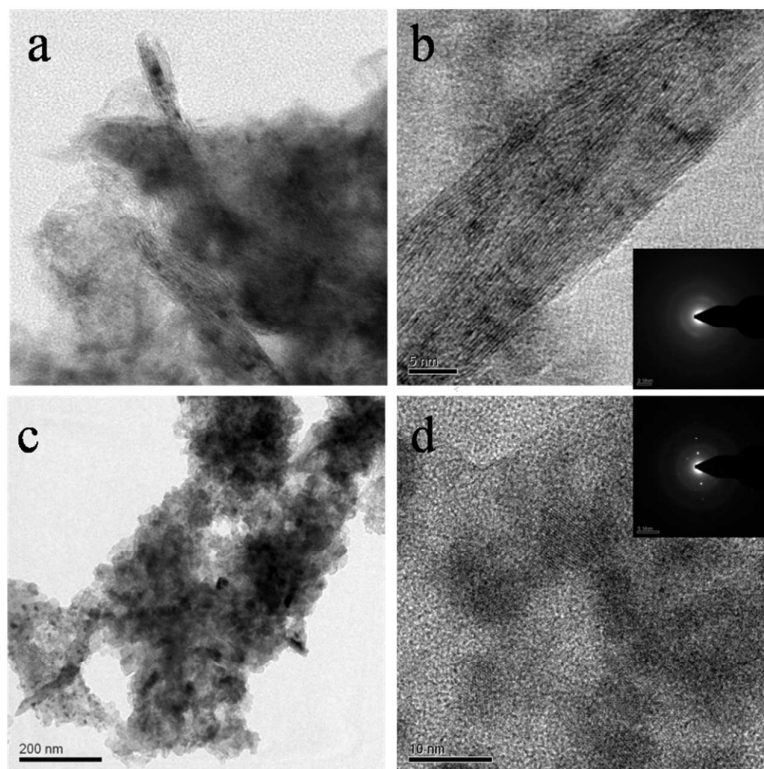


Fig. 6 TEM images of SnO₂NW@GNS electrodes (a) after first charge cycle, (b) HRTEM of nanowire in charged state (inset) SAED pattern and (c) after first discharge cycle, (d) HRTEM and SAED pattern (inset).

